Predicting Fire Season Severity in South America Using Sea Surface Temperature Anomalies

Yang Chen[1], James T. Randerson[1], Douglas C. Morton[2], Ruth S. DeFries[3], George J. Collatz[2], Prasad S. Kasibhatla[4], Louis Giglio[5], Yufang Jin[1] and Miriam Marlier[3]

[1] Department of Earth System Science, University of California, Irvine, CA 92697

[2] NASA Goddard Space Flight Center, Biospheric Sciences Branch, Greenbelt, MD 20771

[3] Department of Ecology, Evolution, and Environmental Biology, Columbia University, New York 10027

[4] Nicholas School of the Environment, Duke University, Durham, NC 27708, USA

[5] Department of Geography, University of Maryland, College Park, MD 20742, USA

One-sentence summary

We show that SST anomalies can predict annual fire season severity in South America, with Oceanic Niño Index predicting severity in the eastern Amazon and Atlantic Multidecadal Oscillation index in southern and southwestern Amazon, enabling forecasts with 3 to 5 month lead times.

Keywords: teleconnection, biomass burning, climate change, drought, forest degradation

Date: 6 June 2011

Corresponding Author:

Yang Chen
Department of Earth System Science
3317 Croul Hall
University of California, Irvine
Irvine, CA 92697-3100
Email: yang.chen@uci.edu
Phone: (949)-824-0597

Abstract

Fires in South America cause forest degradation and contribute to carbon emissions associated with land use change. Here we investigated the relationship between year-to-year changes in satellite-derived estimates of fire activity in South America and sea surface temperature (SST) anomalies. We found that the Oceanic Niño Index (ONI) was correlated with interannual fire activity in the eastern Amazon whereas the Atlantic Multidecadal Oscillation (AMO) index was more closely linked with fires in the southern and southwestern Amazon. Combining these two climate indices, we developed an empirical model that predicted regional annual fire season severity (FSS) with 3-5 month lead times. Our approach provides the foundation for an early warning system for forecasting the vulnerability of Amazon forests to fires, thus enabling more effective management with benefits for mitigation of greenhouse gas and air pollutant emissions.

Deforestation and forest degradation in South America contribute to anthropogenic carbon (C) emissions and global climate change (*1-4*). The net C flux from deforestation and regrowth throughout Latin America (*5*) accounted for nearly a quarter of the global C emissions from land use and land cover change (*4*) in the 1990s. About half of the C emissions from deforestation and forest degradation are associated with fires (*4*). Fire is widely used as an effective and inexpensive means to remove coarse woody debris during the conversion of forests to croplands and pastures, and to limit woody encroachment in existing pastures (*6-7*). Although deforestation rates in Amazonia have declined over the last five years (*8-9*), trends in fires and burned area have not declined by the same amount, possibly as a result of continued burning following initial forest clearing and escaped fires in intact forests from nearby agricultural activities (*10*). Notably, extensive burning in the Brazilian states of Mato Grosso and Pará during 2007 led to the highest fire emissions of any year during 1997-2009 (*11*), highlighting the need to target forest degradation in addition to deforestation for sustained reductions in land use emissions from the region. Projected decreases in Amazon rainfall during the 21st century (*12-13*) may increase the risk of forest fires (*14-15*), with the potential for larger carbon losses and a positive feedback to climate change (*16*). In this context, more effective ways to manage fires are needed for the design of successful climate mitigation and adaptation strategies. Advance information about the likelihood of fires in the dry season allows time to explore and implement management options such as allocation of fire-fighting resources or targeted burning restrictions.

Here we developed a predictive relationship between sea surface temperature (SST) anomalies and annual fire season severity (FSS) in South America that enables forecasts with 3-5 month lead times. A recent study (*17*) has shown that the anomalous local fire activity in western Amazon can be forecast using SSTs from the tropical North Atlantic. Our approach builds on

this work by combining information from both the Pacific and Atlantic and by allowing for spatially varying contributions from these two different drivers. With our model, we were able to successfully predict interannual variability in FSS for several regions. Examination of the temporal and spatial variability of the model parameters and lead times provided new information about the underlying mechanisms enabling these predictions.

High fire years in South America are often associated with an extended dry season and anomalously low levels of precipitation (*18-19*). Previous studies (*18, 20-24*) have shown that precipitation variability in the Amazon is regulated by SSTs in both the Pacific and Atlantic. During the warm phase of El Niño-Southern Oscillation (ENSO), warming of the tropical eastern Pacific surface ocean increases upward atmospheric motion in the region and alters the east-west Walker circulation. As a consequence, precipitation is suppressed over the central and eastern Amazon (*21-22*). Atlantic SSTs also contribute to precipitation variability within the Amazon, with the North Atlantic controls stronger than those from the South Atlantic during the dry season and for the annual mean (*24*). Anomalously warm SSTs over the tropical North Atlantic are believed to cause a northward displacement of Intertropical Convergence Zone (ITCZ), decreasing convection and precipitation during the dry season in the western and southwestern Amazon (*25*). Thus, the most severe droughts observed in the Amazon over the last three decades have occurred when the tropical eastern Pacific and North Atlantic were anomalously warm (*18-19, 23, 25*).

Fire season severity, here defined as the sum of satellite-based active fire counts (FC) in a 9-month period centered at the peak fire month, depends on multiple parameters that influence fuel moisture levels and fire activity in addition to precipitation, including vapor pressure deficits, wind speeds, ignition sources and the intensity and duration of dry season. As a result,

the relationship between FSS and SSTs may not be the same as the relationships between precipitation and SSTs described above.

To develop our empirical model of FSS we used 2001-2009 FC detected by the Moderate Resolution Imaging Spectroradiometer (MODIS) on board NASA's Terra satellite (*26*) along with two climate indices (CIs) constructed from SST anomalies in the eastern tropical Pacific and North Atlantic. The Oceanic Niño Index (ONI) is a 3-month mean SST anomaly in the Niño 3.4 region (5°N-5°S, 120°-170°W) of the Pacific (*27*). The Atlantic Multidecadal Oscillation index (AMO) represents a similar 3-month mean for the North Atlantic (0°-70°N) (*28*). To identify the optimal lead times for using ONI and AMO to predict fires, we separately calculated the correlation between annual sum of FC during the fire season and each of the two CIs for different months prior to the peak fire month (-1~10 month lead times; defined relative to the end of the CI's 3-month SST anomaly averaging interval) in states of Brazil and Bolivia where biomass burning is high (Table 1, Figure S1) and also for 5°×5° regions across the continent (Figure 1).

We defined our empirical predictive model as a linear combination of the two CIs sampled during these months of maximum correlation:

$$FSS_{predicted}(x,t) = a(x) \times ONI[i(x)] + b(x) \times AMO[j(x)] + c(x) \qquad (1)$$

where $FSS_{predicted}$ is the predicted FSS in region x and year t, a is a spatially varying coefficient applied to ONI, b is a spatially varying coefficient applied to AMO, and c is a constant. Coefficients a and b represent the sensitivities of FSS in each region to ONI and AMO, individually. We obtained a, b and c by fitting the observed time series of annual FSS from Terra MODIS during 2001-2009 (9 years; Figure 1c) with ONI and AMO during the same period. ONI

and AMO were sampled during months *i* and *j*, respectively, in each region based on the maximum correlation (either positive or negative) observed for the individual climate indices. The lead times corresponding to *i* and *j* varied spatially and were computed relative to the peak fire month in each region (Figure 1a, 1b and S2) (Materials and methods are available as supporting material on Science Online.).

Fires in the eastern Amazon were more sensitive to ONI while AMO had the largest impacts on FSS in the southern and southwestern Amazon (Figure 1). The AMO influence on fires had distinctive north-south pattern, with correlations switching from strongly positive to strongly negative north of the equator (Figure S2). AMO had a stronger positive correlation with FSS in Rondonia, Pará, El Beni, Amazonas, and Acre, whereas ONI was more closely linked with FSS in Mato Grosso (Table 1, Figure S3). These spatial patterns were broadly consistent with observed relationships between Pacific and Atlantic SST anomalies and precipitation variability within the Amazon (*24*).

Lead times for the two climate indices relative to the peak fire month were relatively consistent across the different states we targeted in our analysis, ranging between 4-6 months for AMO and 3-7 months for ONI for states other than Amazonas (Table 1). Near or at the timing of peak fire month, the relationship between the two climate indices and FSS was considerably weaker (Figure S1). By combining information from both AMO and ONI in our empirical regression model (Equation 1), we were able to explain some of the interannual variability in FSS across South America during 2001-2009 from Terra MODIS (Figure 1d). Notably, high fire years in 2004, 2005, and 2007 had the highest values of AMO during January-March (the period of optimal lead times) whereas low fire years in 2008 and 2009 had the lowest values of AMO (Figure S4).

To verify the model, we compared the model predictions with Terra MODIS FSS from 2010 (this year was not used to develop the model), FSS derived from three other satellites, and carbon emissions from the Global Fire Emissions Database version 3 (GFED3) that integrates 500m burned area and active fires from multiple sources during 1997-2009 (Figure 2). The model predicted a considerable increase in fires in all regions in 2010 (relative to the 2008 and 2009 fire seasons) that was consistent with all of the available satellite observations (Figure 2). Examining the 2010 predictions in more detail for MODIS Terra, the model generated reasonably accurate predictions for Acre and Pará, overestimated fires in Rondonia, Amazonas, and Mato Grosso, and underestimated fires in El Beni (Figure S5). Predictions from the model in the pre-MODIS era compared to FSS from the Visible and Infrared Scanner (VIRS) on board NASA's Tropical Rainfall Measuring Mission (TRMM) (*29*), the Advanced Along Track Scanning Radiometer (ATSR) World Fire Atlas (algorithm 1) (*30*), and GFED3 (*11*) were most robust for states of Rondonia and Mato Grosso (Figures 2, S5, S6 and S7).

The spatial patterns of high and low severity fire seasons across South America varied considerably and were partially captured by the model. In 2010, for example, the model predicted anomalously high levels of fire activity in both the southeastern and southwestern part of the Amazon basin, consistent with the observed pattern from MODIS (Figure 3). In 2007, in contrast, both model estimates and MODIS observations indicated anomalously high fires were distributed primarily in the southeastern part of the basin.

Many different types of fire occur in tropical forest and savanna biomes, including those associated with deforestation for agricultural expansion, forest fires that may have escaped from different agricultural activities, savanna fires that are associated with pasture maintenance, and agricultural waste burning. To examine the potential of developing separate forecasting models

for these different fire types, we conducted two separate analyses. First, within each state we partitioned fires into forest and non-forest components using MODIS-IGBP vegetation classes, and then separately developed empirical models for these two different classes. Second, we investigated the relationship between understory forest fires in Mato Grosso (*31*) and ONI and AMO climate indices. Models derived for the forest component of each state had similar levels of performance (and lead times) compared to non-forest areas (Table S1 and Figure S1), indicating that our approach may be applicable for many of the fires that contribute to forest degradation. For understory forest fires in Mato Grosso during 1999-2008, we found a significant non-linear relationship with AMO for 9-12 month lead times (Figure S8). ONI, in contrast, appeared to have limited use as forecasting variable.

What are the mechanisms that enable fire season forecasts from SSTs with lead times of ~3-5 months for important biomass burning regions in southern hemisphere South America? These time scales are considerably longer than expected for direct atmospheric circulation adjustments to SST anomalies. Further, although SST anomalies vary relatively slowly (and often have relatively long autocorrelation timescales), it is clear from Figure S1 that the relationship between SST anomalies and the annual sum of active fire detections becomes weaker with shorter lead times. As an example, 2006 was a relatively low fire year across much of southern hemisphere South America, even though both AMO and ONI were exceptionally high at the peak of the fire season (Figure S4).

We hypothesize that precipitation levels during the preceding wet season and during the onset of the dry season in forests of southern hemisphere South America act as a key regulator of drought intensity during the subsequent dry season. Evidence supporting this hypothesis comes from analysis of the seasonal distribution of active fires during high and low fire years (Figure

S9). For satellite observations available over the last decade, the midpoint of the fire season occurred earlier during high fire years (Figure S10), likely as a consequence of reduced precipitation during preceding months. This finding also is consistent with the observation that precipitation anomalies 1-4 months before the peak fire month (corresponding to the dry season and wet-to-dry transition season) were more negatively correlated with the annual sum of FC than precipitation anomalies during the peak fire month (Figure S11). The correlation between AMO and precipitation during the wet-to-dry transition period and early dry season was particularly strong for southwestern Amazonia (Figure S12). Patterns of interannual variability in precipitation also indicated that climate at the onset of the dry season was an important controller– standard deviations and coefficients of variation were higher during the wet-to-dry transition period than for the subsequent dry-to-wet transition (Figure S13).

One possible contributing factor for the time delays between SST anomalies and dry season intensity may involve recharge of soil moisture in forests during the wet season. High SST anomalies in the North Atlantic during November-March limit the southward movement of the ITCZ and thus recharge of soil moisture levels in forest ecosystems across the southern Amazon during these months (Figure S12). As a consequence, transpiration rates by trees may be reduced below average during the following dry season with impacts for both surface humidity and precipitation (*3*). The time scales for these forest-mediated interactions are consistent with earlier work documenting deep rooting systems (*32*) and hydraulic redistribution (*33*) required to maintain high levels of evapotranspiration during the dry season (*34*). Further research is needed to improve our understanding of the underlying mechanisms, including the pathways for the atmospheric teleconnections, the strength of transpiration-mediated feedbacks, and the relative

importance of precipitation, temperature, humidity, wind speed, and radiation in regulating fire behavior during the dry season.

Our results demonstrate the potential use of SST anomalies for forecasting of fire season severity. This information may be of use in several different ways to inform mitigation and adaptation strategies (see text S2 in SOM). The relationship between SSTs and fires documented here also provides a new conceptual framework for evaluating future changes in the fire regime across South America. Changes in SSTs in tropical Pacific and Atlantic are driven by both natural oscillations and long term trends caused by global climate change. The AMO has a periodicity of ~76 years (*35*). Given that the most recent warm phase started in the mid-1990s, the warm phase is likely to continue for several more decades, potentially sustaining high levels of fire risk in the southern Amazon. SSTs also respond to forcing from greenhouse gas concentrations and aerosols. If aerosol emissions continue to decrease in the industrialized north, North Atlantic region will warm more rapidly than the South Atlantic (e.g., large AMO) in the future (*25*), leading to higher probability of severe fire seasons. Severe droughts in South America also may occur more frequently during the latter half of the 21st century as a result of climate change (*12, 36-37*), further increasing the need to develop forecasting approaches for fire management.

References

1. S. R. Loarie, G. P. Asner, C. B. Field, *Geophysical Research Letters* **36**, L14810 (2009).
2. M. C. Hansen *et al.*, *Proc. Natl. Acad. Sci. U.S.A.* **105**, 9439 (2008).
3. J. Shukla, C. Nobre, P. Sellers, *Science* **247**, 1322 (1990).
4. G. R. van der Werf *et al.*, *Nature Geoscience* **2**, 737 (2009).
5. R. S. DeFries *et al.*, *Proc. Natl. Acad. Sci. U.S.A.* **99**, 14256 (2002).
6. M. A. Cochrane, *Nature* **421**, 913 (2003).
7. D. C. Morton *et al.*, *Global Change Biology* **14**, 2262 (2008).
8. The Amazon Deforestation Monitoring Project (Programa de cálculo do desflorestamento da Amazônia – PRODES). Data available at http://www.obt.inpe.br/prodes/.
9. C. Streck, *Climatic Change* **100**, 389 (2010).
10. L. Aragao, Y. E. Shimabukuro, *Science* **328**, 1275 (2010).
11. G. R. van der Werf *et al.*, *Atmospheric Chemistry and Physics* **10**, 11707 (2010).
12. W. H. Li, R. Fu, R. E. Dickinson, *J. Geophys. Res. Atmos.* **111**, D02111 (2006).
13. Y. Malhi *et al.*, *Proc. Natl. Acad. Sci. U.S.A.* **106**, 20610 (2009).
14. Y. Le Page, G. R. van der Werf, D. C. Morton, J. M. C. Pereira, *J. Geophys. Res. Biogeosciences.* **115**, G03012 (2010).
15. D. M. J. S. Bowman *et al.*, *Science* **324**, 481 (2009).
16. N. Golding, R. Betts, *Global Biogeochem. Cy.* **22**, GB4007 (2008).
17. K. Fernandes *et al.*, *Geophy. Res. Lett.* **in press**, (accepted 2 May 2011).
18. J. A. Marengo *et al.*, *J. Clim.* **21**, 495 (2008).
19. S. L. Lewis, P. M. Brando, O. L. Phillips, G. M. F. van der Heijden, D. Nepstad, *Science* **331**, 554 (2011).

20. S. O. Los, G. J. Collatz, L. Bounoua, P. J. Sellers, C. J. Tucker, *J. Clim.* **14**, 1535 (2001).

21. V. E. Kousky, M. T. Kagano, I. F. A. Cavalcanti, *Tellus A* **36**, 490 (1984).

22. C. F. Ropelewski, M. S. Halpert, *Mon. Weather Rev.* **115**, 1606 (1987).

23. N. Zeng *et al.*, *Environ. Res. Lett.* **3**, 014002 (2008).

24. J. H. Yoon, N. Zeng, *Clim. Dynam.* **34**, 249 (2010).

25. P. M. Cox *et al.*, *Nature* **453**, 212 (2008).

26. C. O. Justice *et al.*, *Remote Sens. Environ.* **83**, 244 (2002).

27. K. E. Trenberth, *B. Am. Meteorol. Soc.* **78**, 2771 (1997).

28. K. E. Trenberth, D. J. Shea, *Geophy. Res. Lett.* **33**, L12704 (2006).

29. L. Giglio, J. D. Kendall, R. Mack, *Int. J. Remote Sens.* **24**, 4505 (2003).

30. O. Arino, S. Plummer, S. Casadio, in *P. ENVISAT Sym. 2007, SP-636*. (ESA, 2007).

31. D. C. Morton *et al.*, *Remote Sens. Environ.* **115**, 7 (2011).

32. D. C. Nepstad *et al.*, *Nature* **372**, 666 (1994).

33. J. E. Lee, R. S. Oliveira, T. E. Dawson, I. Fung, *Proc. Natl. Acad. Sci. U.S.A.* **102**, 17576 (2005).

34. H. R. da Rocha *et al.*, *Ecol. Appl.* **14**, S22 (2004).

35. M. E. Schlesinger, N. Ramankutty, *Nature* **367**, 723 (1994).

36. Y. Malhi *et al.*, *Science* **319**, 169 (2008).

37. P. M. Cox *et al.*, *Theor. Appl. Climatol.* **78**, 137 (2004).

Supporting Online Material

www.sciencemag.org

Texts S1, S2, S3

Tables S1

Figures. S1-S14

References

Acknowledgements

This research was supported by NASA grants NNX08AF64G and NNX10AT83G and the EU Seventh Research Framework Programme (MACC project, contract number 218793). The GFED3 time series is publicly available at www.globalfiredata.org.

Figure captions

Figure 1. (a) Maximum positive correlation between ONI and Terra MODIS FSS derived from 2001-2009 data. (b) Maximum positive correlation between AMO and FSS for the same period. (c) Mean FSS observed by Terra MODIS during 2001-2009. (d) Correlation between predicted FSS from the empirical model (equation 1) and observed FSS by Terra MODIS. The months at which ONI or AMO had largest positive correlation with FSS are provided for each 5°×5° grid cell in panels a and b. Also shown (in the parentheses) are the associated lead times relative to the peak fire month. The months (and the associated lead time) at which the empirical model can be used for FSS prediction are shown in panel d.

Figure 2. Interannual variability of FSS from different satellites (MOD: Terra MODIS for 2001-2010; MYD: Aqua MODIS for 2003-2010; VIRS: TRMM VIRS for 1998-2009; ATSR: ATSR World Fire Atlas algorithm 1 for 1997-2010) and carbon emissions from GFED3 (1997-2009) compared to predictions from the empirical model (equation 1). Note these datasets of FSS are derived from satellite spectroradiometer observations of active fire counts (FC) with widely varying detector sensitivities and spatial resolutions, and therefore they are scaled to allow for more direct comparisons of the interannual variability. The GFED3 estimates for Amazonas were not scaled. Some of the variability in the observations not captured by our predictive model probably can be attributed to directional changes in land use within each region (see SOM text S3).

Figure 3. Annual ONI and AMO anomalies for 2001-2010 averaged during February-April (the months at which both ONI and AMO had large positive correlations with FSS in high fire states of southern hemisphere South America). The annual FSS anomalies observed by Terra MODIS

and derived from this study were shown for representative high (2005, 2007, 2010) and low (2001, 2008, 2009) fire years. All anomaly values are relative to the 2001-2009 means.

Tables

Table 1. The empirical fire model and validation statistics in different high fire states in South America.

State	Peak fire month	Climate index – annual FSS relationship[1]				Empirical model[2]					Validation[3]			
		lead time (months)		*r*		lead time	model parameters			*r*	*r*			
		ONI	AMO	ONI	AMO		*a*	*b*	*c*	MOD	MYD	VIRS	ATSR	GFED3
Amazonas	Sep	10	4	0.30	0.73	4	0.88	53.8	14.0	0.74	0.70	0.64	0.15	0.53
Pará	Aug	3	5	0.59	0.79	3	47.2	292.9	146.4	0.84	0.82	0.76	0.57	0.52
Rondonia	Sep	7	5	0.62	0.88	5	87.6	1507	334.1	0.73	0.45	0.91	0.58	0.78
Mato Grosso	Sep	5	6	0.82	0.73	5	307.1	1101	516.9	0.75	0.75	0.74	0.69	0.74
El Beni	Sep	3	5	0.43	0.75	3	140.5	974.8	335.4	0.82	0.89	0.42	0.49	0.41
Acre	Sep	7	4	0.43	0.73	4	6.68	185.3	43.9	0.82	0.85	0.72	0.52	0.73

[1] Linear regressions between FSS (the annual sum of active fire counts during the fire season) recorded by Terra MODIS (MOD) and climate indices (CI: either ONI or AMO) with different lead times (number of months prior to the peak fire month) were performed for 2001-2009. The maximum positive correlations (*r*) and the associated lead times (with a cutoff of at least 3 months) are shown. Lead times are computed as the difference between the month of climate index and the peak fire month. Since the climate index is a 3 month mean SST anomaly, we report the lead time relative to the end of the 3-month CI interval (not the center month) to give a more accurate description of the amount of time potentially available to develop a fire season severity forecast.

[2] ONI and AMO values (2001-2009) that have maximum correlations with FSS were used to derive the empirical model using two-variable linear regressions. *a*, *b*, and *c* are coefficients of the formula (equation 1). The lead time describes the number of months before peak fire season for which the empirical model can be used for FSS prediction (and is the smaller of the two CI lead times). *r* is the correlation between predicted and MODIS observed FSS for 2001-2009.

[3] We validated the empirical model by comparing the predicted FSS with observed FSS from MODIS on board Aqua satellite (MYD, 2003-2010), Visible and Infrared Scanner on board Tropical Rainfall Measuring Mission (TRMM) satellite (VIRS, 1998-2009), European Space Agency (ESA) Advanced Along Track Scanning Radiometer World Fire Atlas (ATSR, 1997-2010, algorithm 1), and fire emissions from Global Fire Emission Database version 3 (GFED3, 1997-2009).

(a) max positive corr. between ONI and FSS

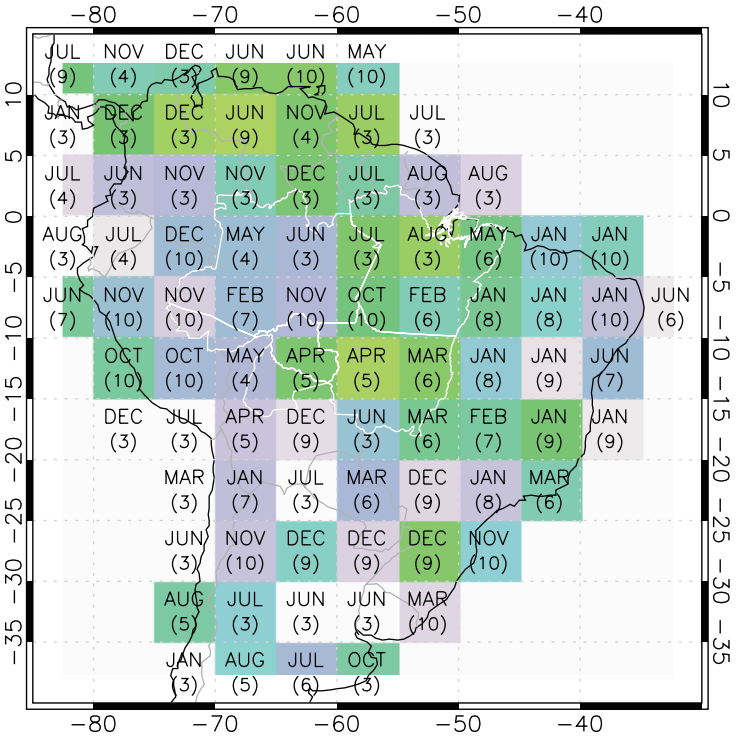

(b) max positive corr. between AMO and FSS

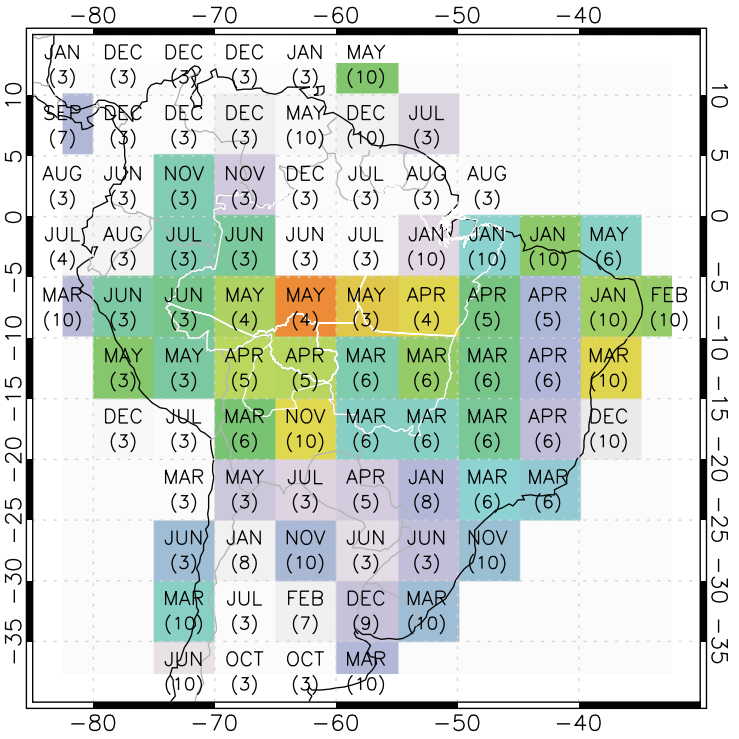

(c) MOD FSS (# $Mha^{-1}yr^{-1}$)

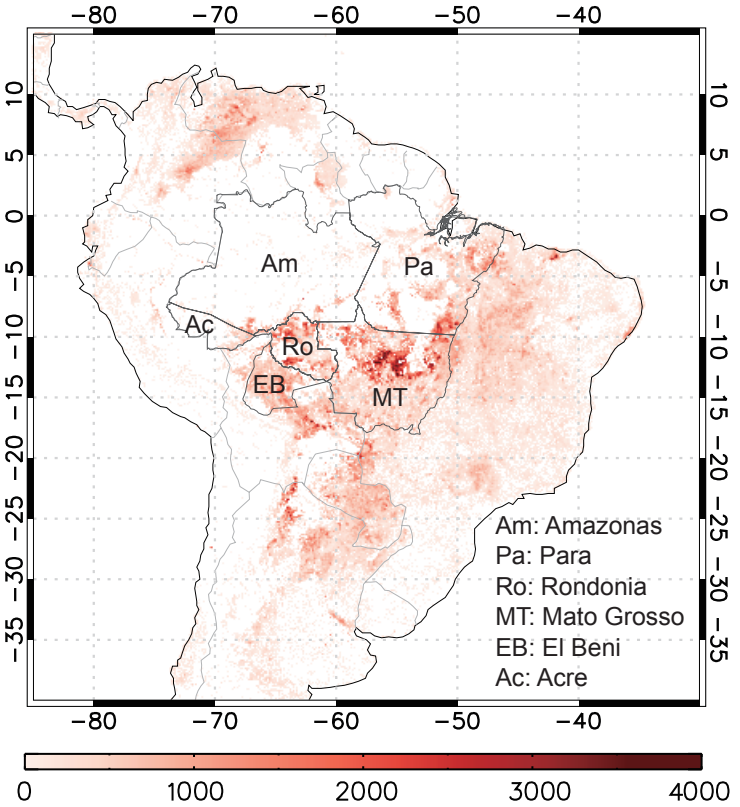

(d) corr. between predicted and MOD FSS

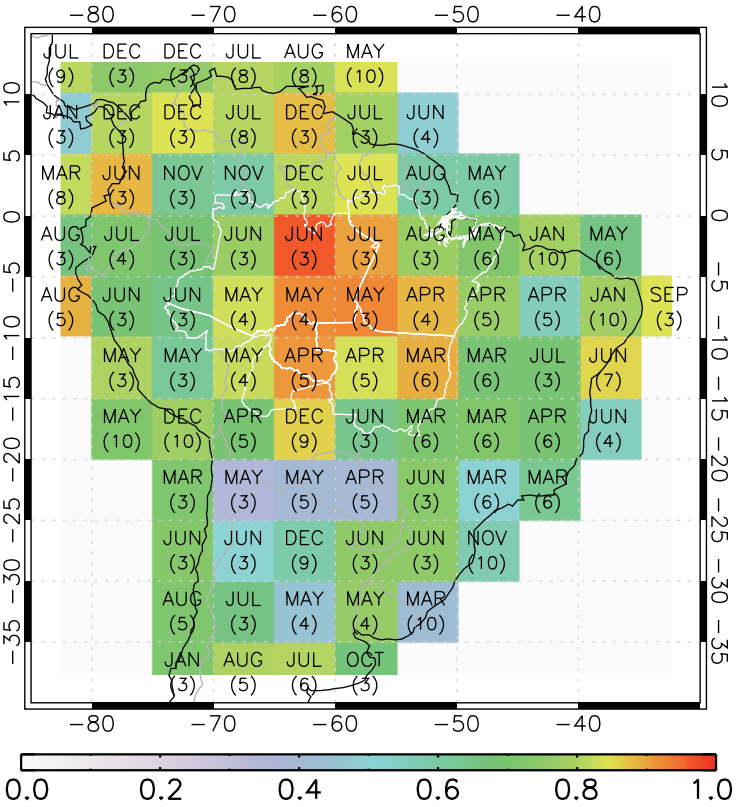

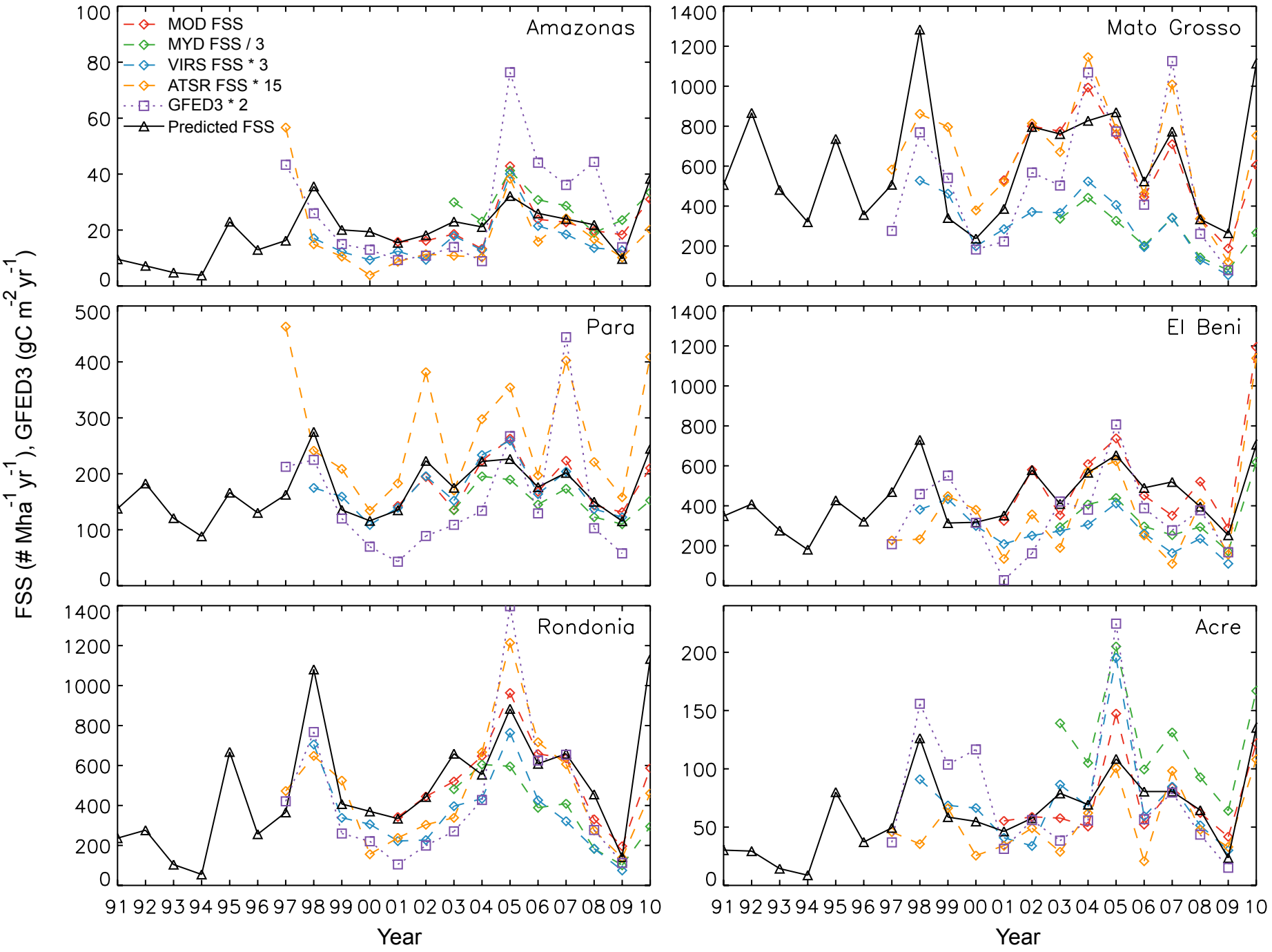
MOD FSS
MYD FSS / 3
VIRS FSS * 3
ATSR FSS * 15
GFED3 * 2
Predicted FSS
Amazonas
Mato Grosso
Para
El Beni
Rondonia
Acre
FSS (# Mha-1 yr-1), GFED3 (gC m-2 yr-1)
Year
Year
91 92 93 94 95 96 97 98 99 00 01 02 03 04 05 06 07 08 09 10

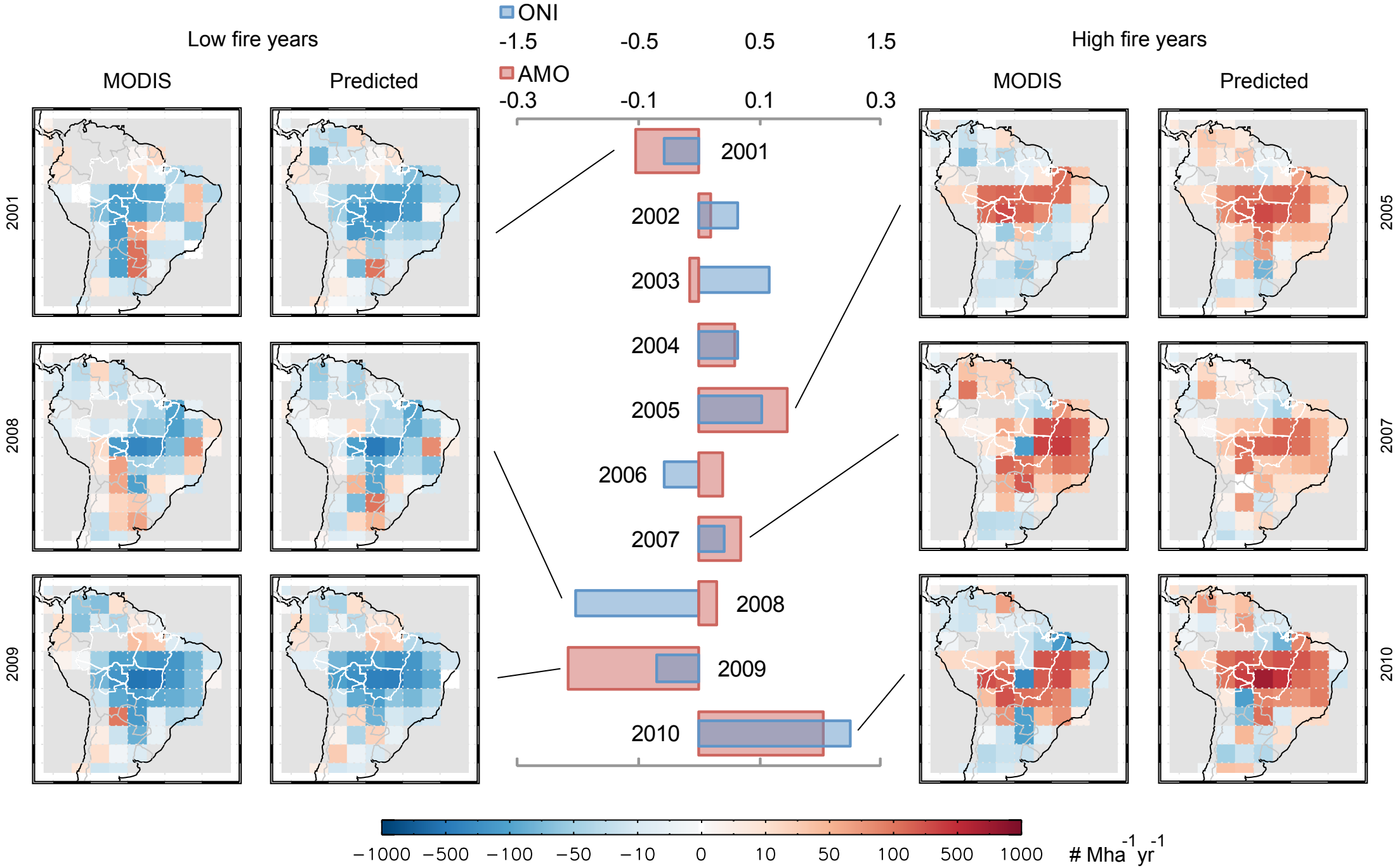
Low fire years
High fire years
MODIS
Predicted
MODIS
Predicted
ONI
-1.5
-0.5
0.5
1.5
AMO
-0.3
-0.1
0.1
0.3
2001
2002
2003
2004
2005
2006
2007
2008
2009
2010
2001
2008
2009
2005
2007
2010
−1000
−500
−100
−50
−10
0
10
50
100
500
1000
Mha-1 yr-1

Supporting Online Material

for paper titled

"*Predicting Fire Season Severity in South America Using Sea Surface Temperature Anomalies*"

by

Yang Chen, James T. Randerson, Douglas C. Morton, Ruth S. DeFries, George J. Collatz, Prasad S. Kasibhatla, Louis Giglio, Yufang Jin and Miriam Marlier

Table of Contents

Text S1. Data and Method

The derivation of coefficients for the fire season severity (FSS) empirical model (Equation 1) was based on active fire counts (FC) detected by the MODIS sensor on board the Terra Satellite during 2001-2009. Specifically, we used MODIS collection 5 global monthly fire location product (MCD14ML, available online at http://modis-fire.umd.edu/AF_getdata.html). We sampled the geographic coordinates of individual fire pixels (at a 1×1 km spatial resolution) that had a confidence level greater than 30%, and calculated the monthly FC within each 0.5° pixel after applying a cloud fraction correction. Persistent hot spots from MODIS observations (*1*) and gas flare pixels in NOAA Global Gas Flare Estimates (*2*) were excluded because the burning in these pixels were mainly associated with petroleum production rather than vegetation fires. We then calculated the monthly FC for each 5°×5° grid cell and for 6 states (Amazonas, Pará, Rondonia, Mato Grosso, and Acre in Brazil and El Beni in Bolivia) that had high levels of deforestation and biomass burning fire emissions in recent years. The sum of FC during the fire season (defined as the 9-month period centered at the peak fire month) was recorded as the annual FSS for each region (either for each 5°×5° grid cell or for each state).

We obtained the Oceanic Niño Index (ONI) time series from the NOAA National Weather Service Climate Prediction Center (http://www.cpc.noaa.gov/) and the Atlantic Multi-decadal Oscillation (AMO) index time series from the NOAA Earth System Research Laboratory website (http://www.esrl.noaa.gov/).

We first performed linear regressions between FSS and the two climate indices (CIs, either ONI or AMO) for different lead times before the peak fire month. Since the CI is a 3 month mean SST anomaly, we report the lead time relative to the end of the 3-month CI interval (not the center month) to give a more accurate description of the amount of time potentially available to develop a fire season severity forecast. For most regions, 9 years of data (2001-2009) were used for the regression. For some regions where the peak fire month was during or before April, only 8 years of data (2002-2009) were used. These regions occurred mostly north of the equator, for example in Venezuela and Columbia. For each region, the month for which the CI had maximum positive or negative correlations with FSS was recorded (individually for ONI and AMO). If the maximum positive correlation was higher than the absolute value of the maximum negative correlation, we used the CI values for the month with maximum positive correlation. To predict FSS at or before the beginning of the fire season, we established a cutoff (minimum) lead time of 3 months. We then used the ONI and AMO values (sampled during the months when the correlation between the CI and FSS was at a maximum) to derive the coefficients (a, b, and c) for each region. This was done by performing a two-variable linear regression following the form of Equation (1) in the main text.

Data used to validate the empirical model include active fire counts observed by the Terra MODIS (MOD) in 2010, active fire counts observed by the MODIS on board the Aqua satellite (MYD) for 2003-2010, active fire counts observed by Tropical Rainfall Measuring Mission (TRMM) Visible and Infrared Scanner (VIR) for 1998-2009, active fire counts from European

Space Agency (ESA) Advanced Along Track Scanning Radiometer World Fire Atlas (ATSR, algorithm1) for 1997-2010, and fire emissions for 1997-2009 from the Global Fire Emission Database version 3 (GFED3). MODIS-IGBP vegetation classes from the MODIS 500m land cover product (MOD12Q1, collection 4, for the year 2001-2004) were used to partition the forest and non-forest regions of each state. We separately calculated FSS and developed empirical models for these two different classes.

Using the precipitation rate (PPT) from TRMM 3B43 dataset (available online at http://disc.sci.gsfc.nasa.gov/index.shtml), we performed linear regressions between FSS and PPT with variable lead times. The results for the 6 states with high levels of biomass burning are shown in Figure S11. We also explored the correlations between TRMM PPT for 4 seasonal periods and the CI values sampled at different months (see Figure S12).

Text S2. Use of fire season severity in mitigation and adaptation strategies

Using the method given in this paper to forecast FSS will be of use in several different ways to inform mitigation and adaptation strategies. For example, investment in fire management could be strengthened in places vulnerable to fire damage before the onset of high severity fire seasons– with lead times of 3-5 months enabling investment in personnel and infrastructure. Even larger lead times may be possible in some regions with only slightly reduced forecasting skill (Figure S14). Given the potential damage caused by fires that escape from pasture maintenance and land clearing activities into nearby forests, permitting systems for these forms of land management could be modified to reduce risks, on a state by state basis. Forecasts may also be useful for assessing the success of fire management, including for example using the predicted versus actual fire season severity, to evaluate avoided carbon emissions. One important use of these forecasts may involve mitigating public health impacts from exposure to degraded air quality during severe fire seasons (*3*), since fire emissions can directly contribute to the global burden of disease due to outdoor air pollution (*4*). Fine particulate matter and ozone emissions from fires are of special concern for patients with susceptibilities to cardiovascular or respiratory disease (*5*-*6*).

Text S3. Methodological uncertainties

The relationship between fire activity and precipitation can be highly non-linear (*7*). Fuel moisture control on fire season severity varies in different ecosystems, and often decreases in savanna and grassland ecosystems where fire spread rates may be limited by the availability of fine fuels (*8*). Additional factors, including economic drivers (*9*) and policy decisions regarding land management (*10*) influence the fire regime, and likely contribute to some of the variability that we cannot explain with the simple empirical model described in this paper. For example, our method overestimated the fire season intensity in 2007 and 2010 over a 5×5 grid cell (60°W-

55°W, 15°S-10°S) in western Mato Grosso (Figure 3), where very high levels of deforestation occurred during 2002-2005 *(11)*.

Table S1. The empirical fire model and validation statistics for forest (F) and non-forest (NF) regions in different high fire states in South America. Non-forest fractions in Amazonas and Acre were smaller than 10% and so we did not partition the all-vegetation model (Table 1) into F and NF components for these states.

State	Biome	CI-FSS correlations				Empirical model					Validation			
		lead time		*r*		lead	model parameters			*r*	*r*			
		ONI	AMO	ONI	AMO	time	*a*	*b*	*c*	MOD	MYD	VIRS	ATSR	GFED3
Para	F	3	8	0.54	0.81	3	41.1	275.8	115.3	0.86	0.94	0.77	0.39	0.46
	NF	4	5	0.47	0.53	4	56.6	363.9	235.0	0.60	0.88	0.75	0.47	0.57
Rondonia	F	7	6	0.59	0.89	6	93.2	1893	374.7	0.93	0.47	0.88	0.54	0.69
	NF	5	5	0.76	0.79	5	124.0	625.3	232.5	0.93	0.51	0.81	0.61	0.87
Mato	F	5	4	0.84	0.76	4	456.7	1708	684.2	0.94	0.65	0.73	0.59	0.62
Grosso	NF	5	6	0.64	0.54	5	162.7	514.0	355.4	0.70	0.86	0.61	0.69	0.79
El Beni	F	3	6	0.09	0.73	3	-23.0	744.3	175.1	0.74	0.62	0.58	0.45	0.54
	NF	3	5	0.56	0.72	3	275.7	1268	488.5	0.87	0.92	0.36	0.46	0.39

Figure S1. Correlation coefficients between FSS and CIs (either ONI or AMO) for different lead times (number of months prior to the peak fire month). The months with highest positive correlation (with a cutoff of at least 3 month lead time) are highlighted with filled circles. The correlation coefficients are separately shown for all, forest, and non-forest vegetation classes in 6 high-fire states in South America. Non-forest fractions in Amazonas and Acre were smaller than 10%, so the correlations in these two states are shown only for the all-vegetation class. The dashed lines represent levels of $p = 0.02$ and $p = 0.05$ for a two-tailed test.

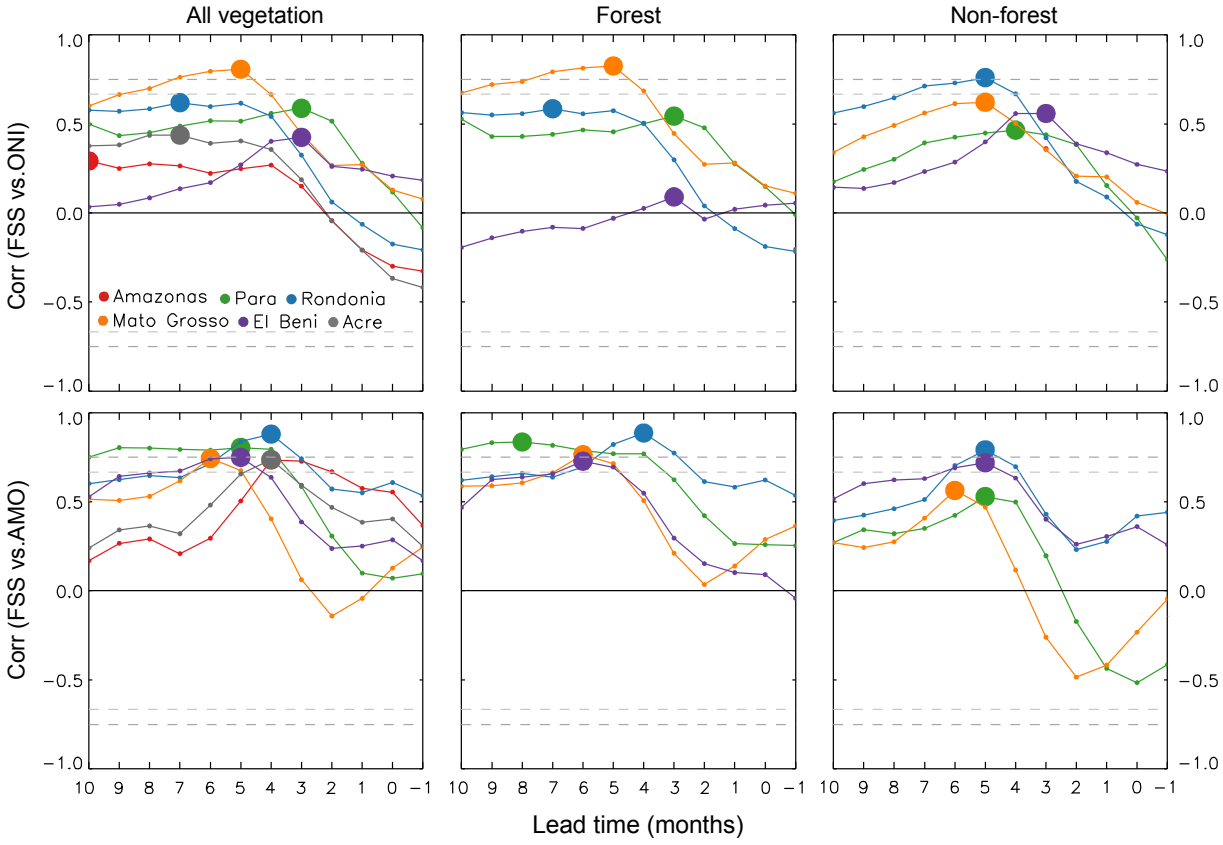

Figure S2. Same as Figure 1a and 1b, but for the maximum negative correlations between FSS and the two CIs.

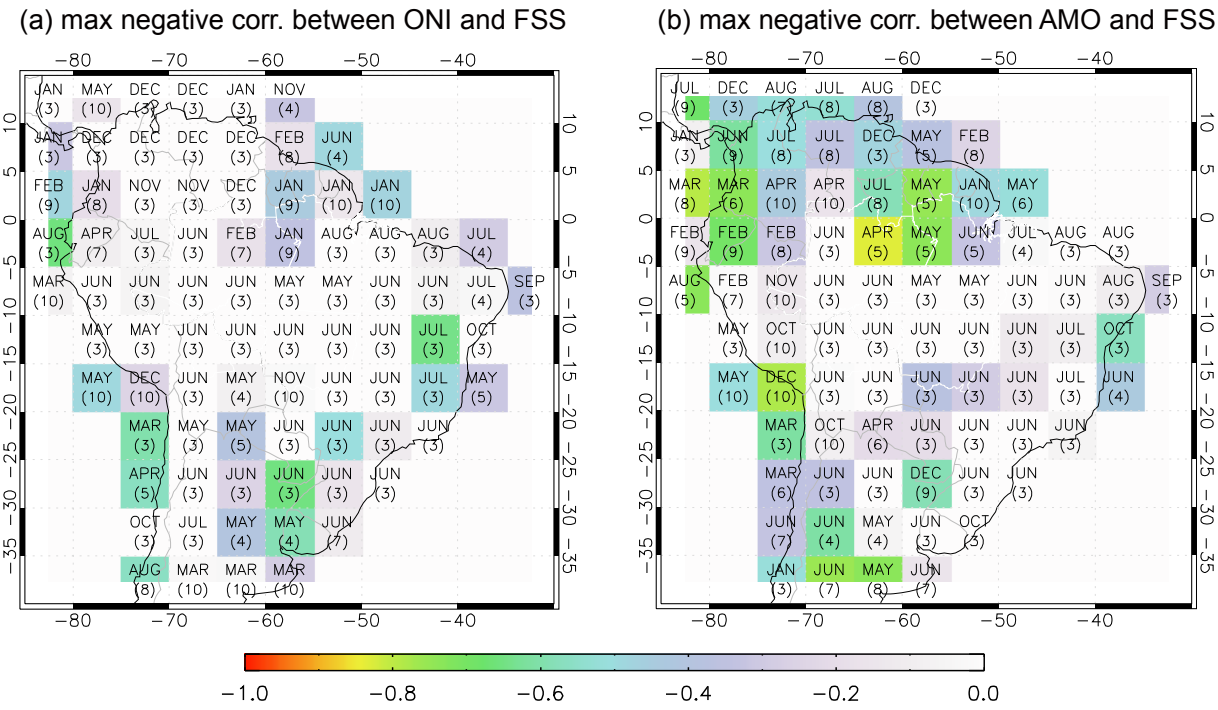

Figure S3. Scatter plots of FSS versus ONI or AMO for months with highest positive correlation. The last digit of each year is shown within each circle (2001-2009).

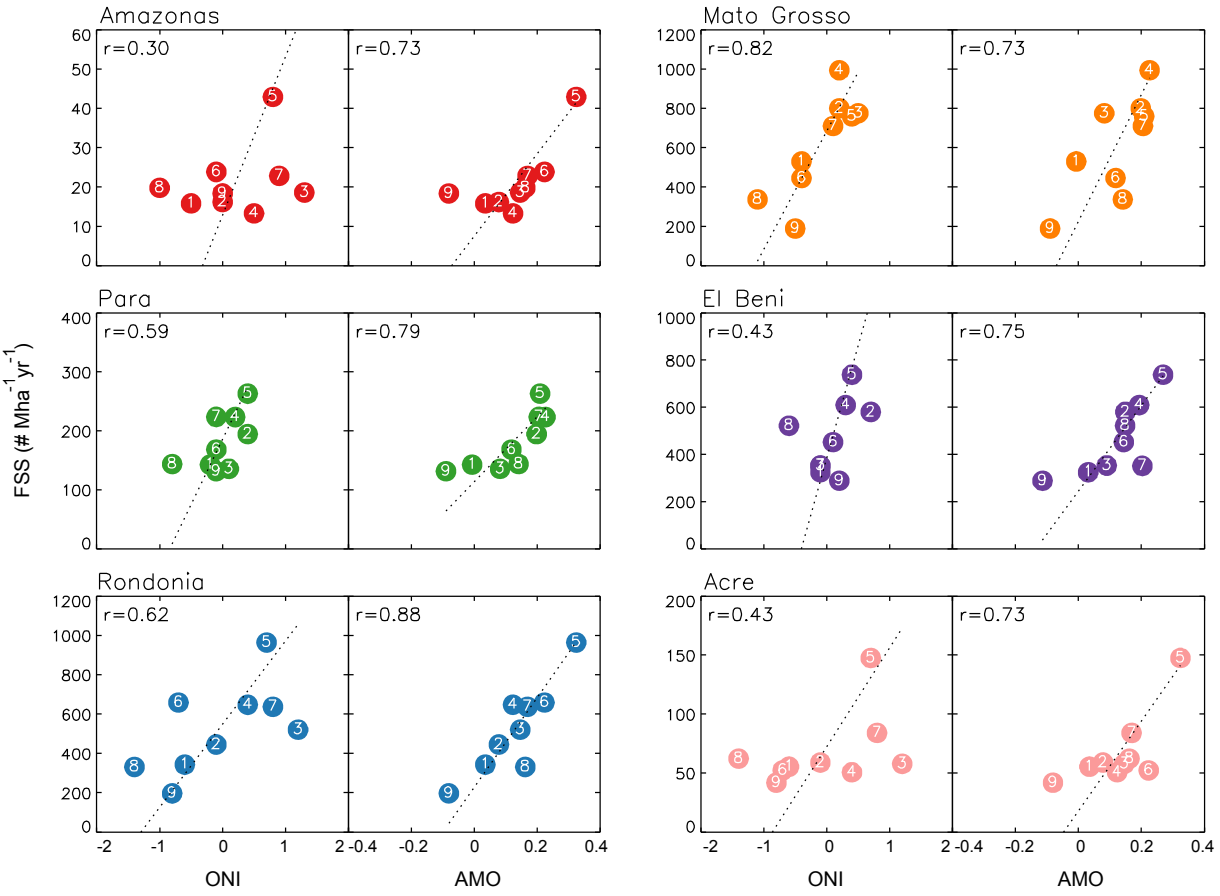

Figure S4. Time series (2001-2009) of monthly ONI and AMO, along with total FC in South America and in 6 states of Brazil and Bolivia. The black dots indicate the month at which ONI or AMO had largest positive correlation with the sum of annual FC during the fire season in Mato Grosso.

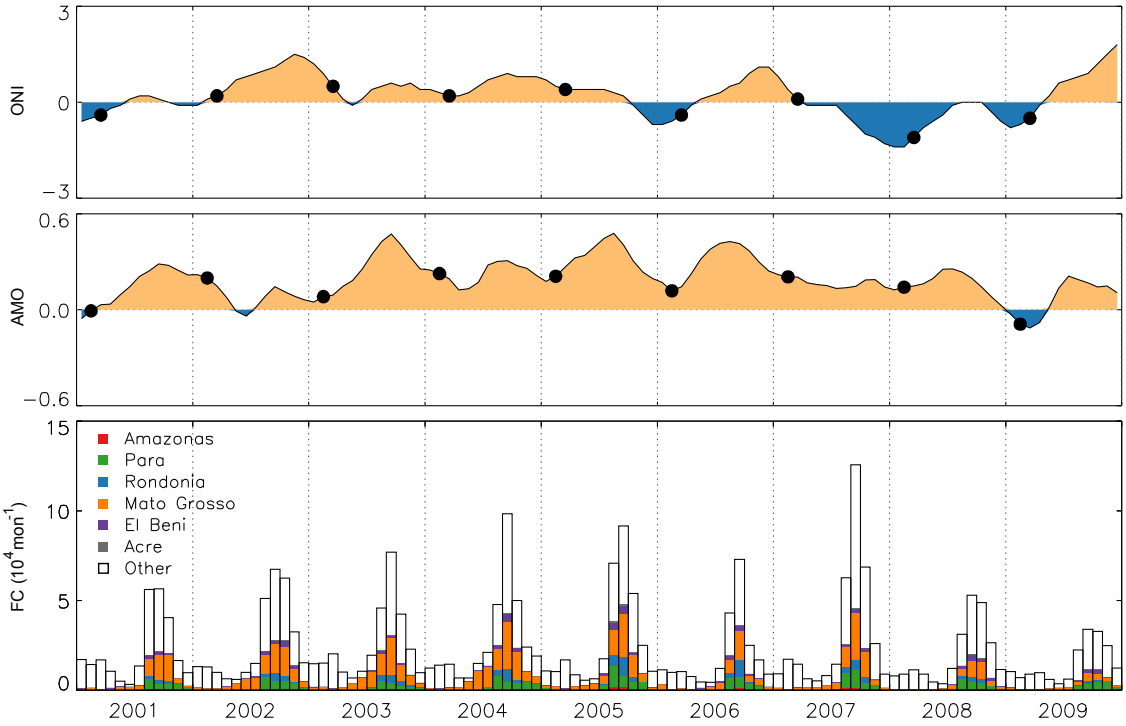

Figure S5. Scatter plots of predicted annual MOD FSS (derived from Terra MODIS FC data for 2001-2009) versus FSS detected by satellites (MOD: Terra MODIS for 2001-2010; MYD: Aqua MODIS for 2003-2010; VIRS: TRMM VIRS for 1998-2009; ATSR: ATSR World Fire Atlas algorithm 1 for 1997-2010) and fire emissions from GFED3 (1997-2009). Open circles represent data during 2001-2009 (the period used to derive the empirical model) and closed circles represent data for other years that are (2010 for MOD and MYD; 1998-2000 for VIRS; 1997-2000 and 2010 for ATSR, and 1997-2000 for GFED3).

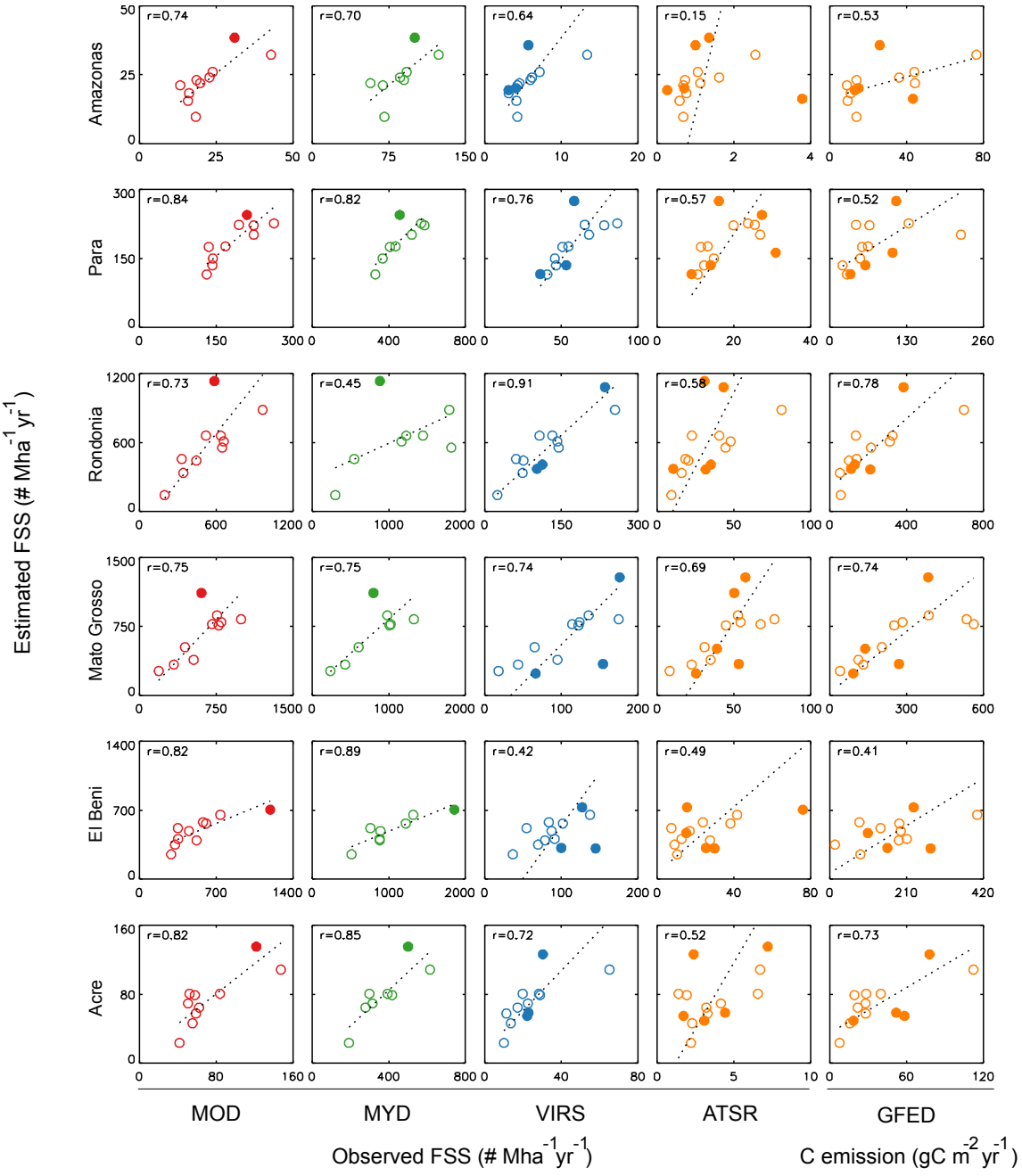

Figure S6. (a) Fire C emissions (averaged over 1997-2009) from GFED version 3; (b) correlation between predicted FSS and GFED3 emissions.

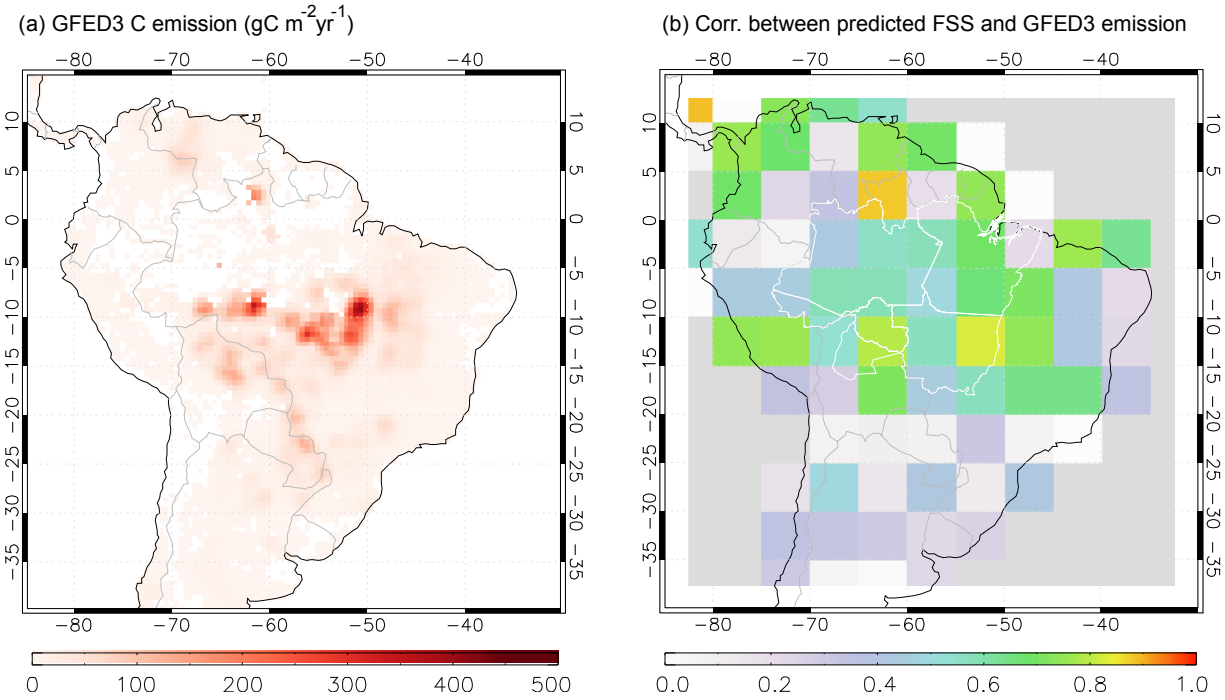

Figure S7. Maps of correlations between predicted FSS (using either combined method as given in Equation 1, or methods based on single variable regressions between FSS and ONI/AMO) and FSS detected by satellites (MOD for 2001-2010; MYD for 2003-2010; VIRS for 1998-2009; ATSR for 1997-2010) and fire emissions from GFED3 (1997-2009).

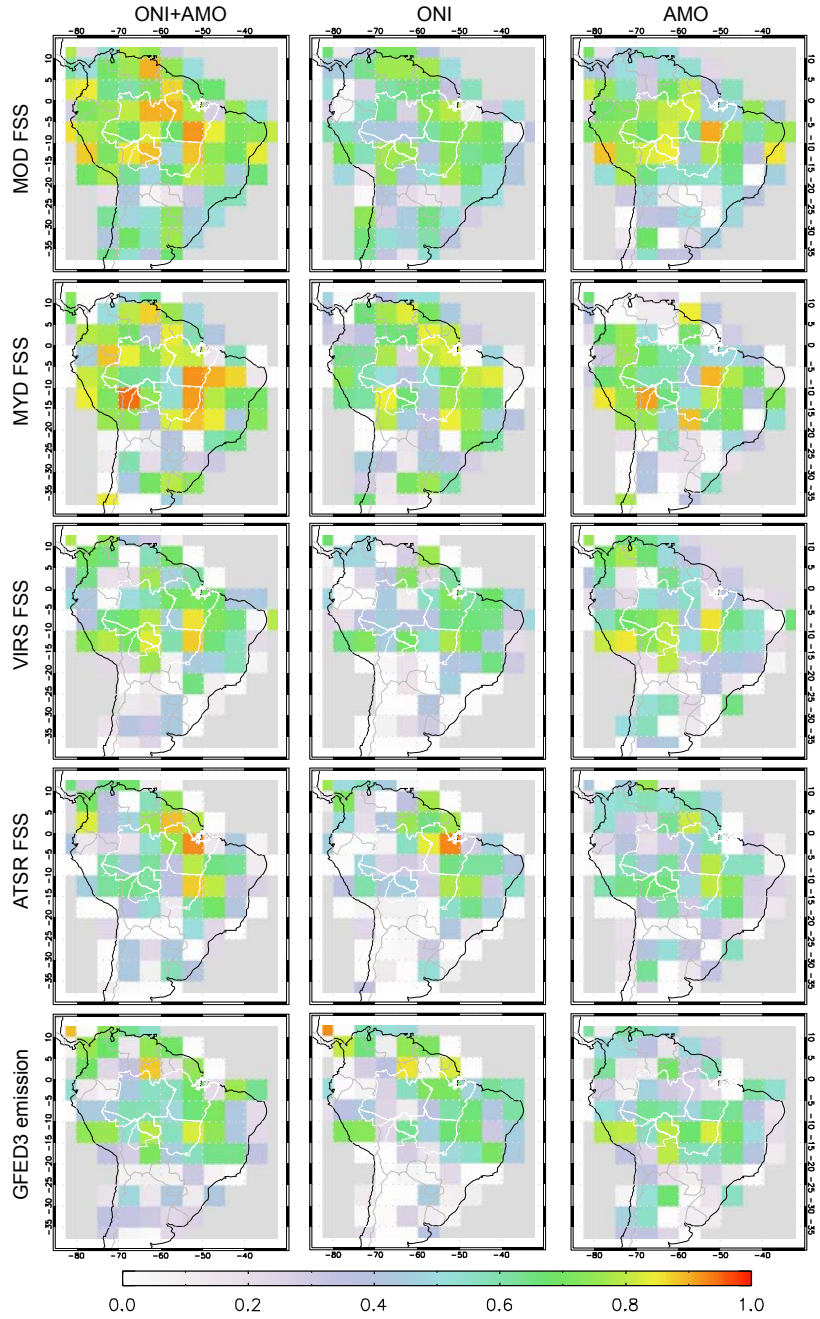

Figure S8. Correlation between CIs and the burned area of understory fires in Mato Grosso during 1999-2008 with different lead times (*lt*). The last two digits of the years are shown in circles. The annual extent of understory forest fire damages was estimated from 2000-2010 MODIS data, using methods described in (*12*). An exponential fit line between AMO and burned area is shown for each panel with *lt* between 9 and 12 months. The last two digits of the years are shown within the circles.

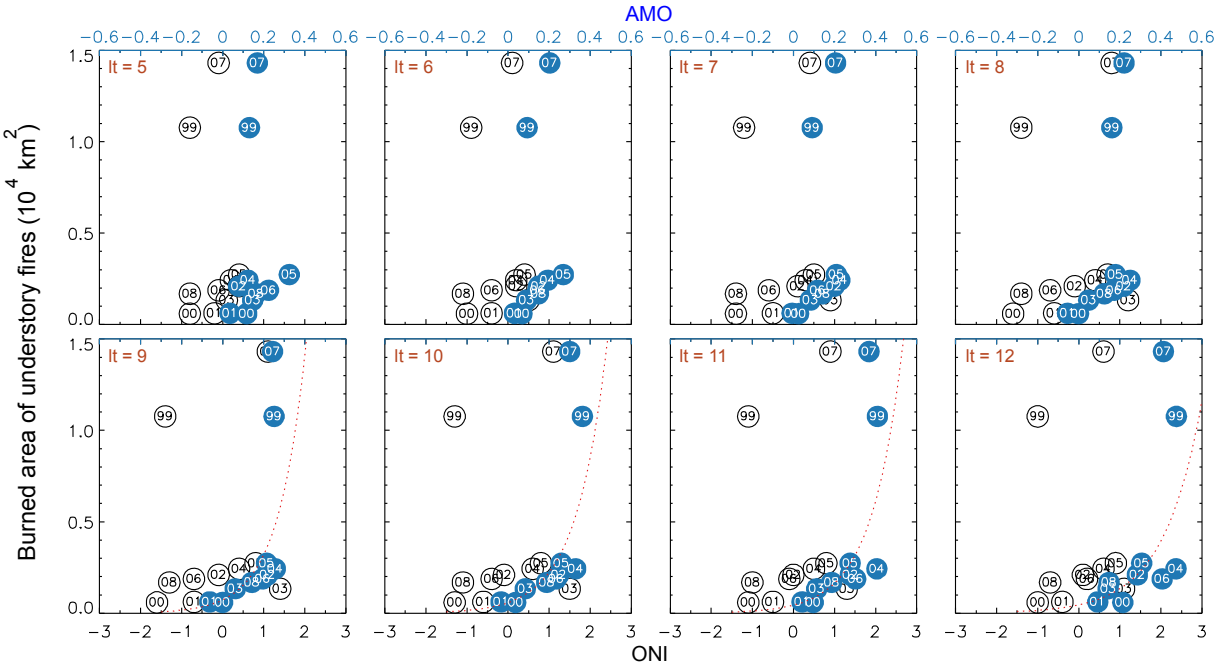

Figure S9. (a) Monthly distributions of Terra (MOD) FC for each year between 2001 and 2009, and the 2001-2009 mean. (b) Normalized (monthly FC divided by annual FC) monthly distributions of FC.

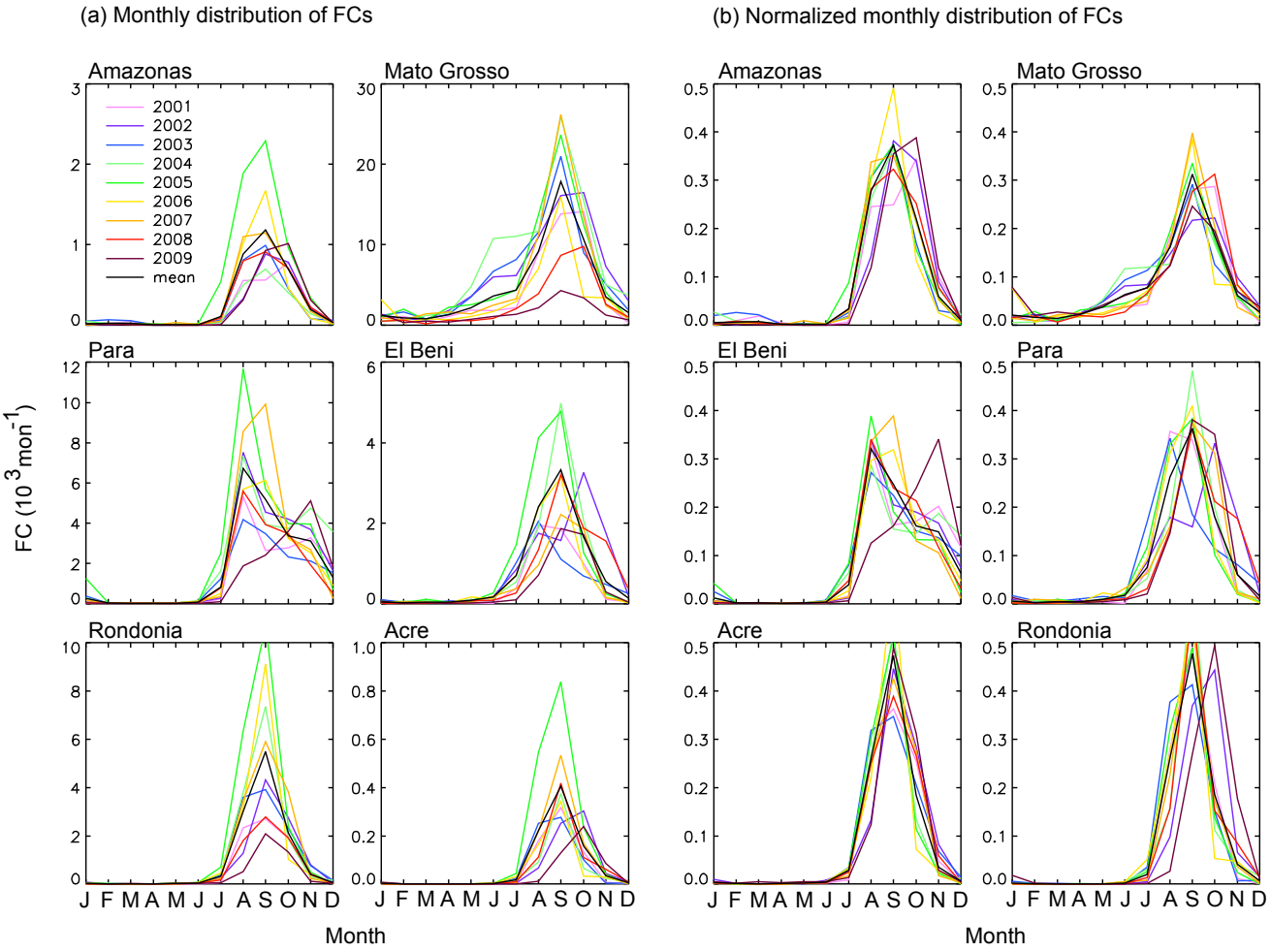

Figure S10. The midpoint of the fire season shown as a function of annual FC observed by Terra MODIS (MOD, 2001-2010), Aqua MODIS (MYD, 2003-2010), TRMM VIRS (1998-2009), and ATSR World Fire Atlas algorithm 1 (1997-2010). The midpoint of the fire season was estimated as the center point of a FC-weighted temporal distribution using all active fires observed by Terra MODIS during each year (March-March). The last two digits of the years are shown in circles.

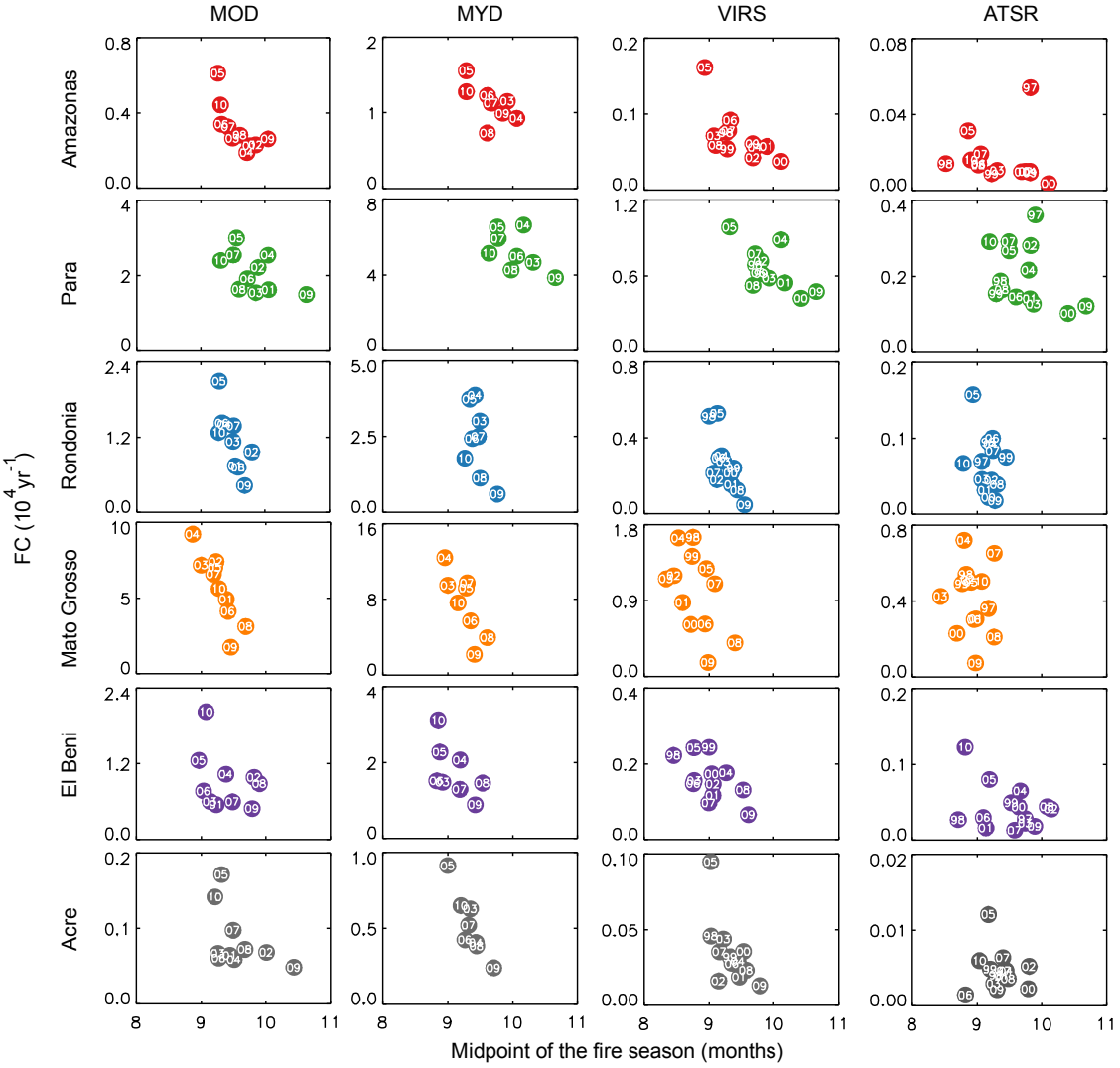

Figure S11. Correlation coefficients (r) from linear regressions between FSS and the mean precipitation rate during 3-month moving windows with variable lead times (months before the peak fire month). Dashed lines indicate levels of $p = 0.02$ and $p = 0.05$ for the two-tail significance test.

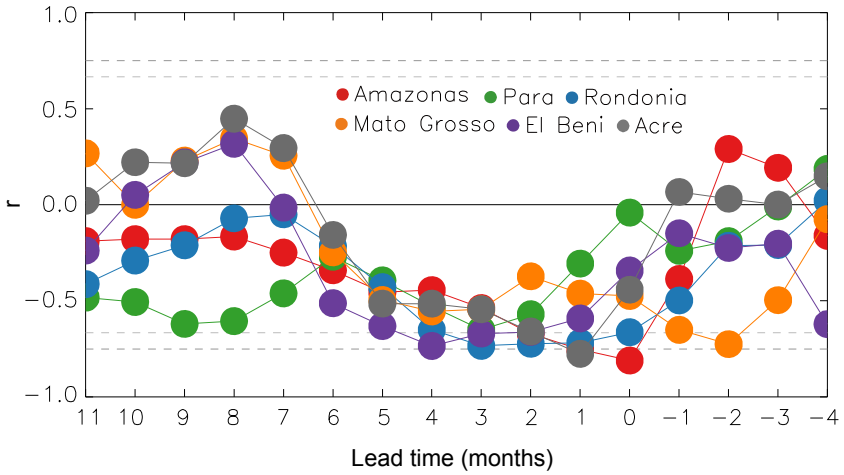

Figure S12. Mean precipitation rates (from TRMM 3B43 dataset, averaged over 1998-2010) during different seasons (left most column) and their correlation with CI (either ONI or AMO) sampled during different months (following 12 columns). For months after the end of each season (e.g., after Aug for JJA; marked below each panel), ONI and AMO data sampled from the previous year were used to estimate the correlation. These results show that AMO had large impacts on precipitation in western and southwestern Amazon during both dry season and the wet-to-dry transition with 2-4 month lead times. The relationship between ONI and precipitation in the dry season was considerably weaker, but ONI may influence the fire season intensity in eastern Amazon by impacting the precipitation rate during the wet-to-dry transition.

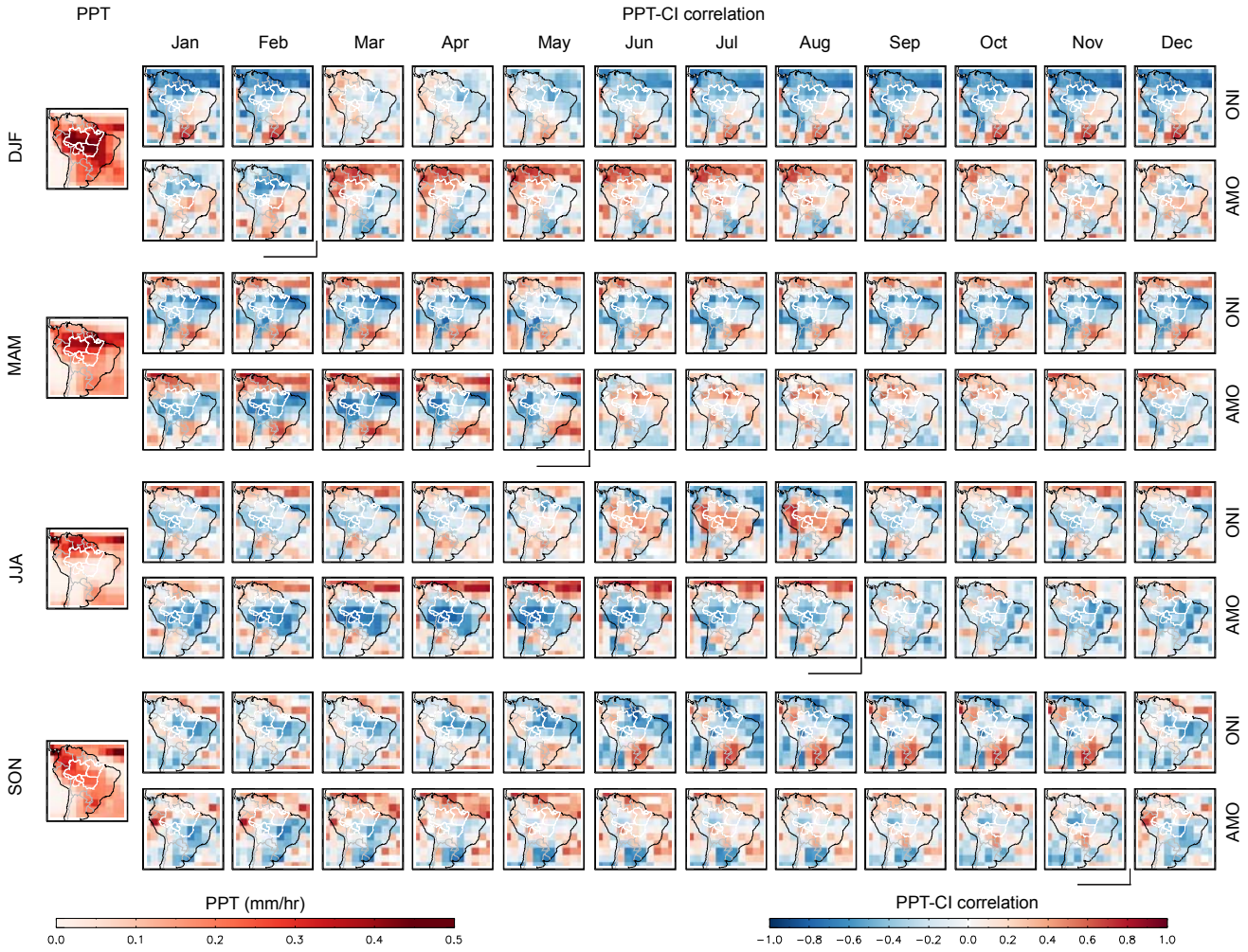

Figure 13. Monthly means of precipitation rate (PPT) with error bars, relative standard deviation (σ) of PPT, and FC. The PPT data were 1998-2010 averages from TRMM 3B43 dataset. The FC data were from Terra MODIS observations (averaged during 2001-2010).

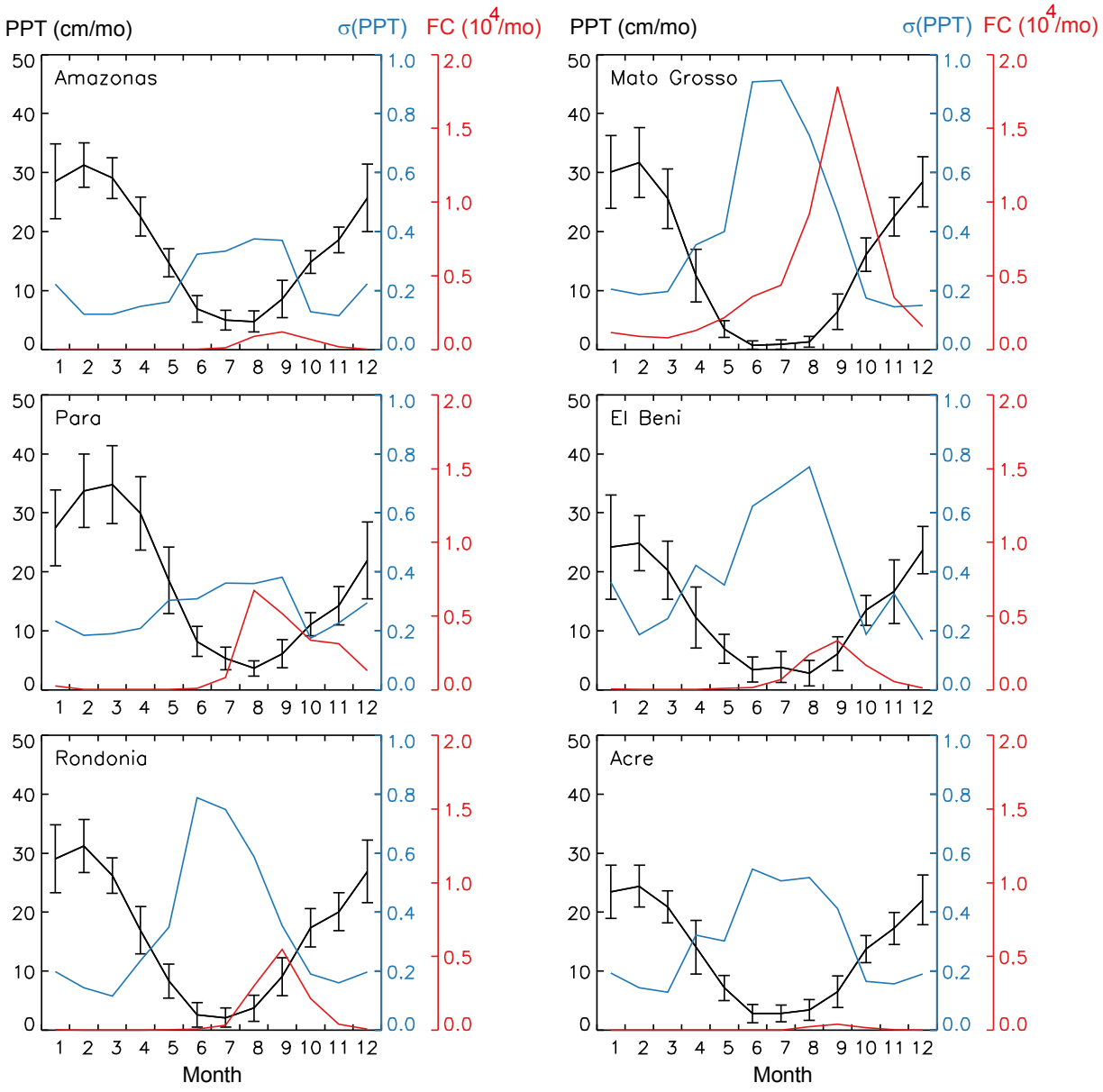

Figure 14. Correlations between observed FSS and FSS predicted using SST anomaly data with larger lead times. The rightmost points for each state represent estimates using ONI and AMO sampled during months with optimized lead times (with a 3-month cutoff lead time that is the same as that given in Table 1 of the main text).

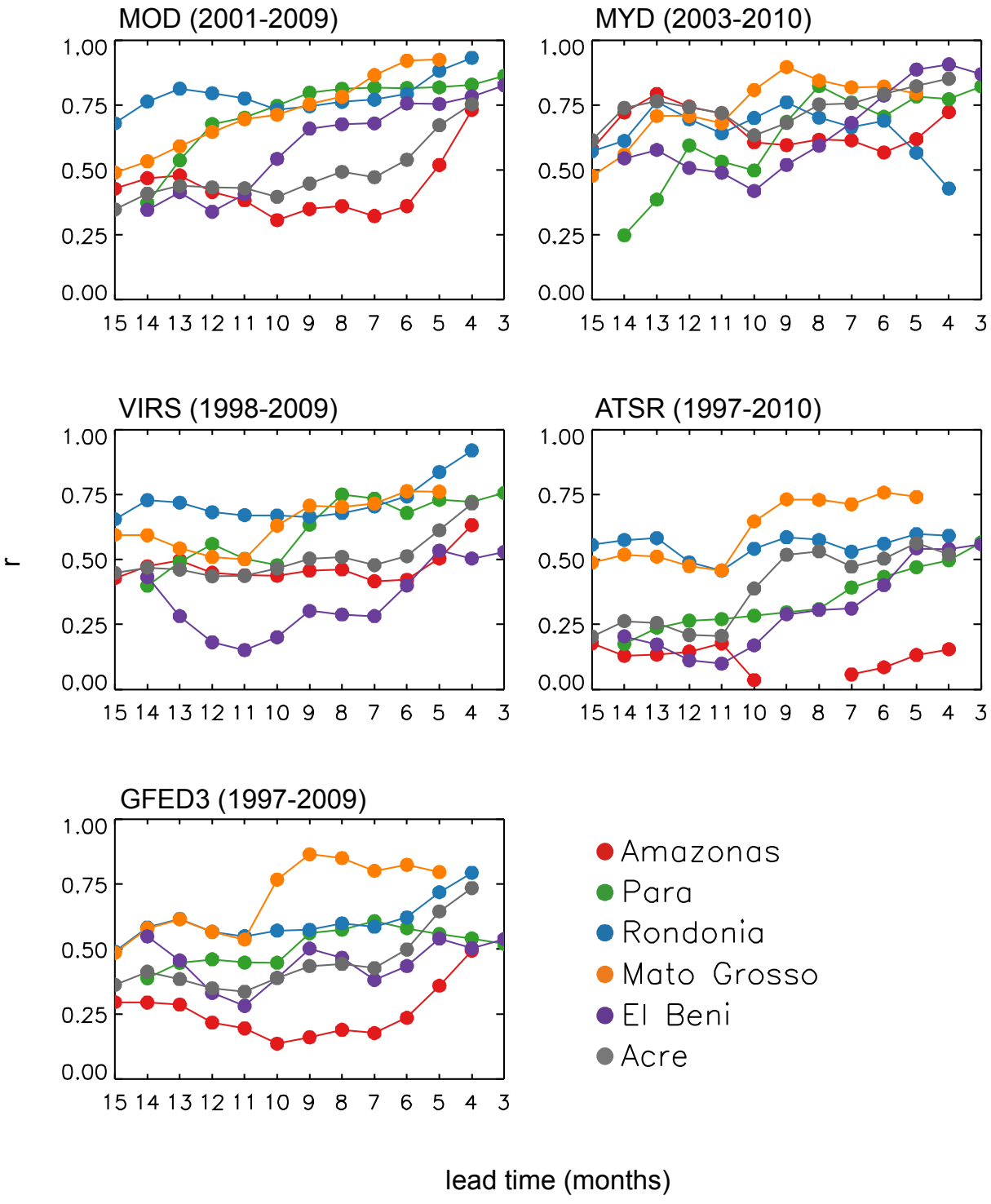

References

1. L. Giglio, I. Csiszar, C. O. Justice, *Journal of Geophysical Research-Biogeosciences* **111**, (2006).
2. C. D. Elvidge *et al.*, *Energies* **2**, 595 (2009).
3. B. Langmann, B. Duncan, C. Textor, J. Trentmann, G. R. van der Werf, *Atmospheric Environment* **43**, 107 (2009).
4. S. C. Anenberg, L. W. Horowitz, D. Q. Tong, J. J. West, *Environ Health Persp* **118**, 1189 (2010).
5. C. N. do Carmo *et al.*, *Rev Panam Salud Publ* **27**, 10 (2010).
6. J. S. Lighty, J. M. Veranth, A. F. Sarofim, *J Air Waste Manage* **50**, 1565 (2000).
7. G. R. van der Werf *et al.*, *Proceedings of the National Academy of Sciences of the United States of America* **105**, 20350 (2008).
8. J. T. Randerson *et al.*, *Global Biogeochemical Cycles* **19**, 2 (2005).
9. D. C. Morton *et al.*, *Global Change Biology* **14**, 2262 (2008).
10. C. Streck, *Climatic Change* **100**, 389 (2010).
11. The Amazon Deforestation Monitoring Project (Programa de cálculo do desflorestamento da Amazônia – PRODES). Data available at http://www.obt.inpe.br/prodes/.
12. D. C. Morton *et al.*, *Remote Sensing of Environment*, **115**, 7 (2011).